PAPER

A facile synthesis of Zn-doped TiO$_2$ nanoparticles with highly exposed (001) facets for enhanced photocatalytic performance

Kun Jiang,[ab] Jin Zhang,[b] Rui Luo,[b] Yingfei Wan,[b] Zengjian Liu[b] and Jinwei Chen (ID) *[b]

It is a great challenge to simultaneously improve the visible light absorption capacity and enhance photon-generated carrier separation efficiency of photocatalysts. Herein, Zn-doped TiO$_2$ nanoparticles with high exposure of the (001) crystal face were prepared *via* a one-step hydrothermal decomposition method. A detailed analysis reveals that the electronic structures were modulated by Zn doping; thus, the responsive wavelength was extended to 600 nm, which effectively improved the visible light absorption of TiO$_2$. More importantly, the surface heterojunction of TiO$_2$ was created because of the co-existing specific facets of (101) and (001). Therefore, the surface separation efficiency of photogenerated electron and hole pairs was greatly enhanced. So, the optimal TiO$_2$ photocatalyst exhibited excellent photocatalytic activity, in which the Rhodamine B (RhB) degradation efficiency was 98.7% in 60 min, under the irradiation of visible light. This study is expected to provide guidance for the rational design of TiO$_2$ photocatalysts.

1. Introduction

Titanium dioxide (TiO$_2$) has emerged as one of the most promising photocatalysts for the elimination of wastewater pollution due to its excellent properties such as high stability, non-toxicity, low-cost and outstanding photocatalytic activity.[1,2] However, the inherent electronic structure ($C_B = -0.3$ eV, $V_B = +2.9$ eV, $E_g = 3.2$ eV) of TiO$_2$ weakens its utilization efficiency of solar energy.[3,4] More importantly, the short free time and severe surface recombination of photogenerated electrons greatly reduce the efficiency of the photogenerated carriers.[5,6] Therefore, it is urgent to develop some effective strategies to widen the optical capture range and enhance the separation efficiency of photo-generated carriers of TiO$_2$.

It is urgent to modify TiO$_2$ with extended visible light absorption and increased visible light activities. Elemental doping is an effective method to modulate the electronic structure of TiO$_2$, which decreases the bandgap to enhance the visible light absorption capacity.[7] According to the principle of elemental doping and the structure of TiO$_2$, doping of elements mainly exists in three ways: (1) O atom sites, such as N,[8,9] C,[10] and defects.[11–13] (2) Ti atom sites, such as Fe,[14,15] Cu,[16,17] and Zn,[18] (3) Interstitial doping.[19] Elemental doping can greatly enhanced the visible light absorption of TiO$_2$. However, doped atoms are usually used as carrier recombination centers, which

further weaken the efficiency of photo-generated carrier separation.[20] Hence, how to coordinate the relationship between the photo-generated carrier separation and the visible light absorption of TiO$_2$ is more important.

In order to overcome the above-mentioned obstacles, it is highly desirable to develop a simple and effective strategy to enhance the separation of photo-electrons and hole pairs of TiO$_2$. In general, the construction of heterojunctions or loading transition metal nanoparticles on TiO$_2$ surfaces is an effective strategy to decrease the recombination of photo-electron and hole pairs, which can effectively improve the bulk phase separation efficiency of photogenerated electrons in TiO$_2$.[21,22] In addition, the surface separation of photogenerated electrons plays a crucial role in the photocatalytic reaction. Based on this consideration, researchers found that electrons exhibit anisotropic properties on specific facets of TiO$_2$. For example, the concept of surface heterojunction was proposed by Yu *et al.*[23–25] Under the function of the surface heterojunction, the oriented photogenerated holes migrate to the (001) crystal face and electrons migrate to the (101) crystal face, which greatly inhibited the surface recombination of photogenerated carriers, thus improving the utilization efficiency of photogenerated carriers. Similarly, Liu *et al.* prepared TiO$_2$ with a high density of surface heterojunction and confirmed the existence of surface heterojunction on the TiO$_2$ surface.[26] However, to the best of our knowledge, TiO$_2$ with high exposure of (001) specific facets usually has a poor capability to capture visible light and thus greatly decreased the visible-light photocatalytic activity.

Herein, Zn-doped TiO$_2$ nanoparticles with highly exposed (001) facets are synthesized by a one-step hydrothermal

[a]Department of Integrated Traditional Chinese and Western Medicine, West China Hospital, Sichuan University, Chengdu 610041, PR China

[b]College of Materials Science and Engineering, Sichuan University, Chengdu 610065, PR China. E-mail: jwchen@scu.edu.cn; Tel: +86-28-8541-8786

method. The characteristics and photocatalytic performance of the obtained catalysts are investigated. The results show that Zn doping can effectively modulate the electronic structure of TiO_2, which greatly enhanced the visible light absorption capacity of TiO_2. More importantly, the co-existing specific facets of (101) and (001) on TiO_2 surfaces greatly promote the separation efficiency of photogenerated carriers. Hence, under the synergistic effects of Zn doping and surface heterojunction, the photocatalytic activity of TiO_2 for RhB degradation under visible light was greatly improved.

2. Experimental

2.1 Materials

Titanium(IV) sulfate $Ti(SO_4)_2$ (≥99% purity), zinc fluoride ZnF_2 (≥99% purity) and zinc sulfate $ZnSO_4$ (≥99% purity) were supplied by Aladdin, and were used as titanium and zinc precursors. All the chemical reagents, such as sodium fluoride (NaF) and urea (CH_4N_2O) were of analytic grade. All materials were used without further pretreatment. P25 (TiO_2, Degussa) was purchased for comparison.

2.2 Sample preparation

Zn-doped TiO_2 nanoparticles with high (001) facets were synthesized by a one-step hydrothermal method. A certain amount of $Ti(SO_4)_2$ was dissolved in a DI water solution to configure with 0.5 mol L^{-1} of $Ti(SO_4)_2$ for current work. Then, 9.09 g of CH_4N_2O and a certain amount of a mixture of NaF and ZnF_2 were mixed into a 75 ml $Ti(SO_4)_2$ solution under vigorous stirring until complete dissolution. The obtained solution was placed into a 100 ml Teflon-lined autoclave at 140 °C for 12 h. After cooling to room temperature, the nanoparticles were washed with deionized water and alcohol three times and freeze-dried at −60 °C. The obtained photocatalysts were denoted as x%-Zn-TiO_2(001), where x% represented the Zn/Ti molar ratio. Zn-doped TiO_2 (Zn-TiO_2) was synthesized by the same procedure by replacing the mixture of NaF and ZnF_2 with $ZnSO_4$. TiO_2(001) and TiO_2 were prepared by the same procedure with and without NaF, respectively. For comparison, P25 was used as the commercial reference material.

2.3 Characterization

XRD patterns were obtained on a Rigaku XRD Ultimate IV using Cu Kα radiation (λ = 0.154 nm) at a scanning range of 5–85°. The morphological properties were determined using a transmission electron microscope (TEM, Tecnai G2 F20, FEI Co., USA). The X-ray photoelectron spectrometer (XPS) was used to characterize the surface information of the composite (Escalab 250Xi, TMO, USA). A spectrophotometer (UV3600) was used to record the ultraviolet-visible diffusing reflection spectrometry patterns of the specimens. Electron spin resonance (ESR, JES FA200, JEOL) was employed to detect the transient radical intermediates.

2.4 Catalytic activity test

Rhodamine B (RhB) was employed to evaluate the photocatalytic performance of the as-prepared samples under visible

irradiation. First, RhB solution and TiO_2 photocatalysts were prepared. Second, 50 mg each of the TiO_2 photocatalyst was dispersed in 100 ml RhB solution (20 mg L^{-1}) individually at 20 °C in a jacketed glass reactor. Third, the obtained solution was fiercely stirred for 60 min in a dark environment for achieving adsorption–desorption equilibrium. Then, the solution was illuminated by a xenon lamp with a power of 300 W and an optical filter (λ > 420 nm, AM = 1.5) was used to cut off the ultraviolet light. The distance between the solution and the light source was 10 cm. At last, 4 ml solution was extracted during the process of degradation every 20 min centrifuged at 14 000 rpm for 5 min and examined via UV-vis spectrophotometry. The individual absorption peak of rhodamine B at 554 nm was used to determine its concentration in the solution. The degradation efficiency of RhB was calculated using the following equation.

$$\text{Degradation rate } \% = \frac{(C_0 - C_t)}{C_0} \times 100\%$$

where C_0 and C_t are the initial and equilibrium concentrations of RhB, respectively.

3. Results and discussion

3.1 Characterization of the photocatalysts

Morphological information including the size, shape and crystalline interplanar spacing of the as-prepared photocatalysts was acquired via TEM and HRTEM. TEM and HRTEM images of Zn-TiO_2(001) are shown in Fig. 1. The results of Fig. 1(a) and (b) show that Zn-TiO_2(001) nanoparticles have a foursquare shape with an average size of 40 nm. It has been reported that the foursquare shape particle exhibits a large percentage of (001) facets. Fig. 1(c) and (d) are the HRTEM images of Zn-TiO_2(001). On the surface of square-shaped particles, the inter-planar distance of 0.236 nm can be attributed to (001) atomic planes and the inter-planar distance of 0.35 nm can be attributed to
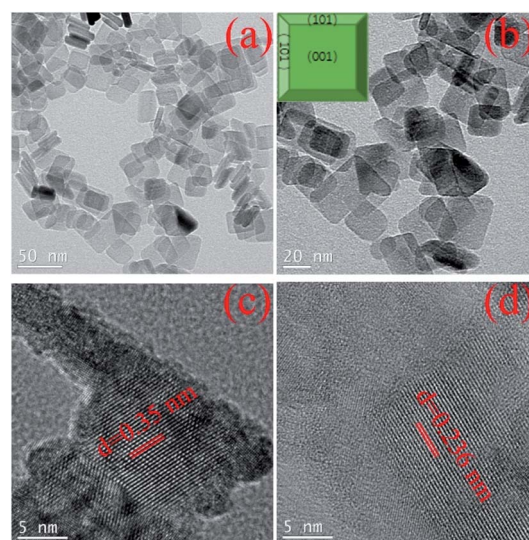

Fig. 1 TEM image of (a and b) Zn–TiO_2(001), (c and d) HR-TEM images of Zn-TiO_2(001).

(101) atomic planes.[26,27] It can be seen from Fig. 1(c) and (d) that the fluorinated photocatalyst exposes a high percentage of (001) facets.

The crystalline structure of the as-synthesized photocatalysts is investigated by XRD. For all TiO_2 samples, as shown in Fig. 2, it can be clearly observed that the characteristic peaks match perfectly with the standard peaks of the anatase phase (JCPDS no. 21-1272) without peaks of other crystalline forms. This result proves that the as-prepared TiO_2 has a high purity of the anatase TiO_2 structure and Zn^{2+} may have been uniformly doped into the lattice of TiO_2 without forming other crystalline phases. To investigate the chemical state of each element in the $TiO_2(001)$ and $Zn-TiO_2(001)$ samples, X-ray photoelectron spectroscopy (XPS) was performed. As shown in Fig. 2(b), the presence of Ti, O, C, Zn and F can be clearly observed through the full spectrum scan of the $Zn-TiO_2(001)$ sample, revealing the formation of $Zn-TiO_2(001)$ nanoparticles. As compared to $Zn-TiO_2(001)$, Fig. 2(b) shows the full spectrum scan of the $TiO_2(001)$ sample, it is obvious that there was no presence of a Zn peak in the full spectrum scan. In addition, the carbon peak is attributed to the residual carbon from the sample and adventitious hydrocarbon from the XPS instrument itself. Furthermore, the doping concentration of Zn was 2.27% from XPS results. According to the results of XPS, we can confirm that Zn is successfully mixed into TiO_2, and the doping concentration is 2.7%.

The XPS peaks of Ti 2p and O 1s for $Zn-TiO_2(001)$ and $TiO_2(001)$ are shown in Fig. 3(a) and (b). Comparison of their high-resolution XPS spectra for Ti 2p (Fig. 3(a)) and O 1s (Fig. 3(b)) regions indicates that the introduction of O_v into $Zn-TiO_2(001)$ results in decreased binding energies for both Ti and O. This is because two additional electrons are left once an oxygen atom is removed from the surface of $Zn-TiO_2(001)$, causing increased electron cloud density around the Ti and O atoms near the O_v sites. Furthermore, in the Zn-2p photoelectron spectra of $Zn-TiO_2(001)$, Zn $2p_{3/2}$ and Zn $2p_{1/2}$ peaks appear at 1021.6 eV and 1044.7 eV, respectively, with the energy splitting of 23.1 eV being a signature of the +2-oxidation state of Zn.[28,29] The above observation can be explained in the light of Zn^{2+} being doped substitutionally in the anatase TiO_2 lattice. As the charge on the dopant ions is lower, the electron cloud of Zn^{2+} experiences a slightly stronger pull from the neighboring Ti^{4+} ions with a higher oxidation potential.[30] Fig. 3(d) shows the high-resolution XPS spectrum of the F 1s region. The measured binding energy is 684.5 eV, which is a typical value for
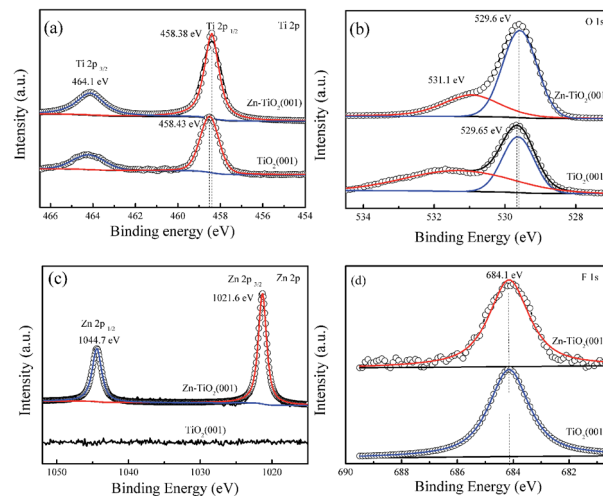

Fig. 3 High-resolution XPS spectra of (a) Ti 2p, (b) O 1s, (c) Zn 2p, and (d) F 1s of $TiO_2(001)$ and $Zn-TiO_2(001)$.

fluorinated TiO_2 systems such as $\equiv Ti-F$ species on the TiO_2 crystal surface. No signal for F^- in the lattice of TiO_2 (BE = 688.5 eV) is found.[31–33]

In order to confirm whether the ZnO was formed on the TiO_2 surface during the hydrothermal process. The surface state of the $Zn-TiO_2(001)$ photocatalyst was determined by Raman spectroscopy, as shown in Fig. 4(a). The peaks at 151.7, 396.5, 516, and 639 cm^{-1} are very close to those reported for anatase. Therefore, the above-mentioned Raman data signify the absence of the ZnO phase and TiF phase in Zn-doped TiO_2 materials. In addition, The N_2 sorption isotherms of P25, $TiO_2(001)$, and $Zn-TiO_2(001)$ samples show a typical curve with the hysteresis loop of the type IV isotherms in Fig. 4(b). The BET surface areas of all samples were calculated. The BET surface
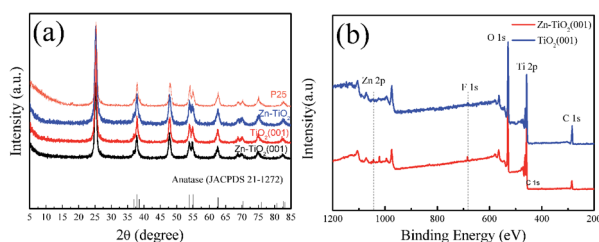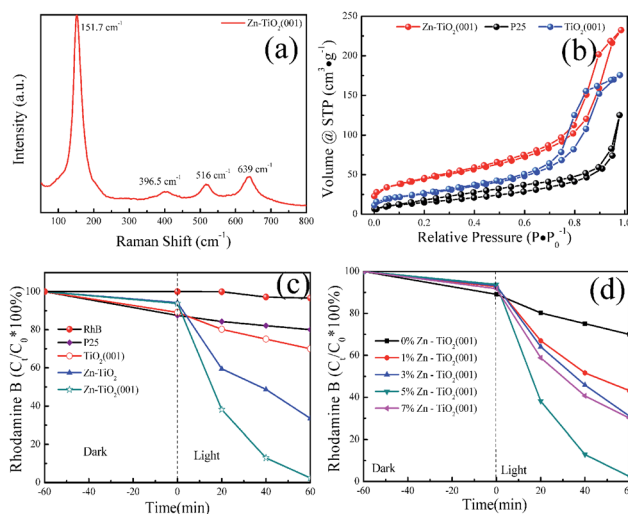

Fig. 4 (a) The Raman scattering spectra of $Zn-TiO_2(001)$, (b) N_2 physisorption isotherms, (c) photocatalytic activity for RhB degradation using different photocatalysts, and (d) photocatalytic activity for RhB degradation using different percentages of Zn doped TiO_2.

Fig. 2 (a) XRD patterns of TiO_2, $Zn-TiO_2$, $TiO_2(001)$ and $Zn-TiO_2(001)$. (b) XPS spectra of $Zn-TiO_2(001)$ and $TiO_2(001)$.

area of P25, TiO$_2$(001), and Zn-TiO$_2$(001) are 56 m^2 g^{-1}, 94.17 m^2 g^{-1}, and 156.7 m^2 g^{-1}, respectively. According to the result of the N$_2$ sorption isotherms, we can speculate that the Zn-TiO$_2$(001) sample may show superior photocatalytic activity because its large surface area could expose more active sites and increase solid–liquid interfaces, which enhance the transportation of photocatalyst-relevant species.

3.2 Photocatalytic performance

The photocatalytic activities of the as-prepared catalysts were evaluated *via* the photo-degradation of RhB under visible-light irradiation. Fig. 4(c) shows the photocatalytic activities of RhB photosensitization P25, TiO$_2$, Zn-TiO$_2$, TiO$_2$(001) and Zn-TiO$_2$(001) samples for RhB degradation under visible-light irradiation. After illumination for 60 min under visible light, around 3.3%, 19% and 20.1% of RhB were removed *via* RhB self-photo-degradation. P25 and TiO$_2$ and TiO$_2$(001) shows higher activity than TiO$_2$ prepared without the F$^-$ based additive. However, the degradation efficiency of RhB is still only around 30%. The doping of Zn seems to show a more pronounced promotion. Zn-TiO$_2$ could remove 65.7% of RhB under 60 min visible light irradiation. Furthermore, 98.7% of RhB was degraded by Zn-TiO$_2$(001), which demonstrates the synthetic effects of Zn doping and high (001) facet exposure for excellent photocatalytic activity under visible light. In order to investigate the effects of the Zn doping concentration on photocatalytic activity, TiO$_2$(001) with different Zn doping concentrations were designed and prepared. As shown in Fig. 4(d), the TiO$_2$-anatase has no obvious effect on RhB degradation under visible light. However, Zn-doped TiO$_2$ samples presented higher photocatalytic activity than TiO$_2$. By increasing the Zn doping amount, the photocatalytic activity of TiO$_2$ was also promoted. When the ratio of Zn to Ti is 0.05, the 5%-Zn-TiO$_2$(001) sample exhibited the highest photocatalytic activity that the degradation efficiency of RhB was 98.7% under 60 min visible light irradiation. Yet, beyond 5% zinc content, the photocatalytic performance of doped Zn-TiO$_2$(001) obviously declined, which may have resulted from the formation of recombination center of photogenerated carriers by the excessive impurity atoms. Based on the literature reported in the last three years, RhB degradation efficiency on different TiO$_2$-based materials is listed in Table 1. In the percent study, RhB degradation with 0.5 g L^{-1} Zn-TiO$_2$(001) is 98.7% in 1 h. This result is higher than that reported for other TiO$_2$-based catalysts.

In addition, the stability of the Zn-TiO$_2$(001) photocatalyst is evidenced by the cycling test, as shown in Fig. 5(a), only a slight
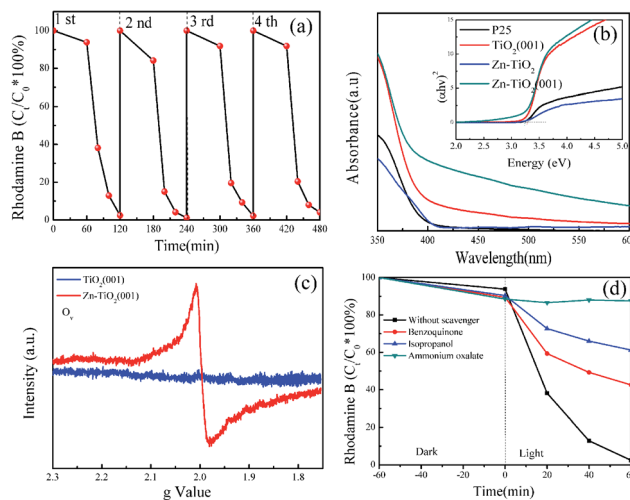

Fig. 5 (a) The reusability of the Zn-TiO$_2$(001) degradation efficiency of RhB under visible light, (b) UV-Vis absorption spectra, band gap energies (inset), (c) ESR signals of O vacancy, and (d) photocatalytic activity of RhB degradation with and without different scavengers.

decrease was observed after 4th cycling. This result shows that the Zn-TiO$_2$(001) catalyst has excellent photochemical stability.

3.3 Mechanism of the enhancement

The light absorption abilities of the as-prepared samples, including P25, Zn-TiO$_2$, TiO$_2$(001) and Zn-TiO$_2$(001), were studied *via* UV-Vis diffuse reflectance spectroscopy. As shown in Fig. 5(b), pure TiO$_2$ (P25) shows a typical absorption band edge at around 375 nm owing to the large band gap of TiO$_2$. Compared with P25, the absorption band edge of TiO$_2$(001) and Zn-TiO$_2$(001) clearly exhibit red-shift and extend to the visible light region. In particular, Zn-TiO$_2$(001) shows the highest response in the visible light range in that the effective adsorption of visible light could extent to 600 nm. The band gaps of P25, Zn-TiO$_2$, TiO$_2$(001) and Zn-TiO$_2$(001) were calculated using the Kubelk–Munk function, as shown in Fig. 5 (b, inset). According to Fig. 5 (b, inset), the band gap of P25 was 3.31 eV. It is consistent with previous research. However, when Zn was introduced into TiO$_2$, the band gap decreased to 3.2 eV and 3.23 eV for Zn-TiO$_2$(001) and Zn-TiO$_2$, respectively. The band gap did not change with Zn doping, so what causes Zn-TiO$_2$(001) sample shows a very strong band tail absorption in the visible-light region (420–600 nm)? According to our previous report, the visible light absorption capacity of a photocatalyst

Table 1 Comparison of RhB degradation efficiencies with different photocatalysts

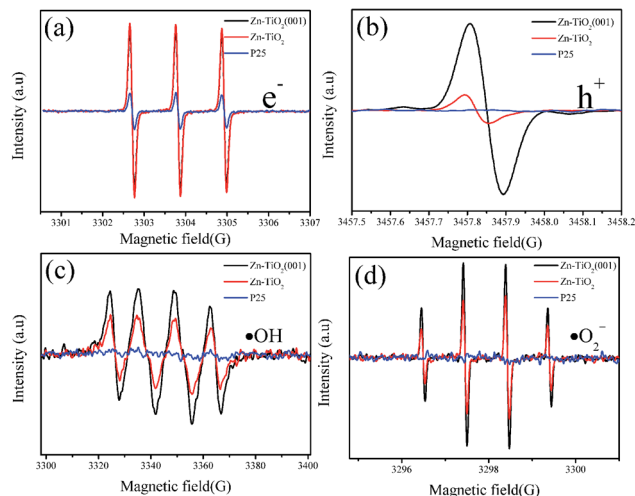| Photocatalyst	Reaction conditions	Degradation efficiency	Ref.
Zn-TiO$_2$(001)	RhB, 20 mg L^{-1}; catalyst, 0.5 g L^{-1}	98.7%, 1 h	This work
Pd/TNTA	RhB, 10 mg L^{-1}; catalyst, 1 g L^{-1}	99.7%, 2 h	34
Tm@Nd@TiO$_2$	RhB, 20 mg L^{-1}; catalyst, 0.5 g L^{-1}	88%, 1.5 h	35
PCN/Fe0(1%)–TiO$_2$	RhB, 10 mg L^{-1}; catalyst, 0.5 g L^{-1}	98%, 1.5 h	36
TiOF$_2$/TiO$_2$	RhB, 20 mg L^{-1}; catalyst, 0.5 g L^{-1}	97.7%, 1.5 h	37

Fig. 6   ESR spectra of P25, Zn-TiO$_2$ and Zn-TiO$_2$(001): (a) e$^-$ under visible light conditions, (b) h$^+$ under visible light conditions, (c) ·O$_2^-$ under visible light conditions and (d) ·OH under visible light conditions.

Fig. 7   The mechanism diagram of Zn-TiO$_2$(001).

was enhanced by defects.[38] Therefore, surface defects on Zn-TiO$_2$(001) were confirmed *via* electron spin resonance (ESR) spectra, as shown in Fig. 5(c). According to previous reports, the characteristics *g* value was 1.998. However, the present ESR studies show almost no presence of Ti^{3+} in the Zn-TiO$_2$(001) photocatalyst. The ESR spectra of Zn-TiO$_2$(001) exhibit a distinct signal at $g = 2.01$ related to the O vacancies of TiO$_2$. Therefore, the ESR data confirm the presence of O-vacancies in Zn-TiO$_2$(001). Under the function of O vacancies, the visible light absorption capacity of Zn-TiO$_2$(001) is greatly enhanced.

Compared to the photocatalytically active substance for degradation in a liquid solution, the existence of a dissolved scavenger is harmful for organic pollutant degradation. The photocatalytic activity is reduced by adding isopropanol (hydroxyl scavenger), ammonium oxalate (hole scavenger), and benzoquinone (superoxide radical scavenger) into the organic solution with visible light irradiation. As shown in Fig. 5(d), the photocatalytic degradation activity of Zn-TiO$_2$(001) has varying degrees of reduction upon the addition of different amounts of scavengers. In particular, after adding ammonium oxalate, the photo-degradation efficiency is reduced to zero, indicating that the photo-generation of hole radicals is critical for the activity substance during the photo-degradation process. It demonstrates that Zn-TiO$_2$(001) with Zn doping and high (001) facets is beneficial for the formation of hole radicals generated on the TiO$_2$ surface.

The ESR spectra were contained to detect the transient radical intermediates in P25, Zn-TiO$_2$ and Zn-TiO$_2$(001). Fig. 6 shows the formation of e$^-$, h$^+$, ·O^{2-} and ·OH after 10 min of visible irradiation under N$_2$ atmosphere. As show in Fig. 6(a) and (b), a strong peak is observed for all catalysts, which are corresponding to the photogenerated of e$^-$ and h$^+$. Compared with P25 and Zn-TiO$_2$, the intensity of the characteristic peak increases with the existence of Zn doping and high (001) facets of Zn-TiO$_2$(001), which implies that doped Zn could promote the photo-generated carrier and the special crystal facet
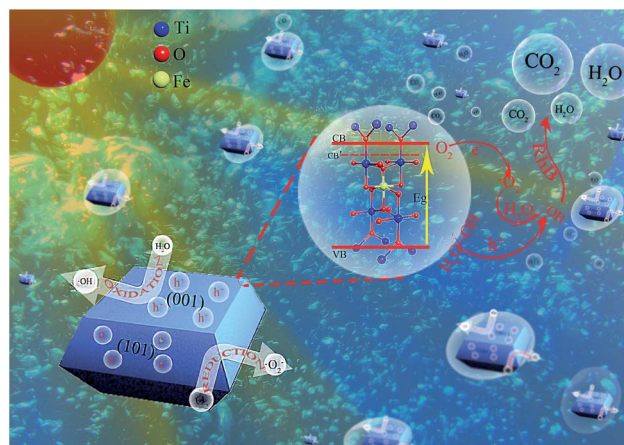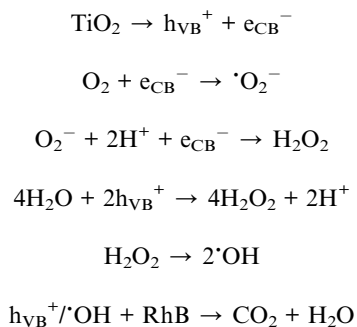
structure could show more holes appearing on the surface of TiO$_2$. Furthermore, as Fig. 6(c) and (d) show, the order of the ·O^{2-} and ·OH radical intensity, both are following Zn-TiO$_2$(001) > Zn-TiO$_2$ > P25 order. It could be concluded that the as-prepared Zn-TiO$_2$(001) photocatalysts could produce more radicals to degrade RhB under visible light. This conclusion is in accordance with the results of the RhB degradation efficiency (Fig. 7).

Based on the experimental data, the mechanism for the improved photocatalytic performance of Zn-TiO$_2$(001) is proposed. The electrons and holes in TiO$_2$ catalysts could be generated under visible light illumination. Then, the electrons in CB and the holes in VB should transfer to the different crystal surfaces of TiO$_2$. During photocatalytic degradation, the main active substance consuming organic pollutants is superoxide radical (·O$_2^-$), hydroxyl radical (·OH), and holes (h$^+$). The mechanism of RhB photo-degradation is proposed as follows:

$$TiO_2 \rightarrow h_{VB}^+ + e_{CB}^-$$

$$O_2 + e_{CB}^- \rightarrow {}^\cdot O_2^-$$

$$O_2^- + 2H^+ + e_{CB}^- \rightarrow H_2O_2$$

$$4H_2O + 2h_{VB}^+ \rightarrow 4H_2O_2 + 2H^+$$

$$H_2O_2 \rightarrow 2{}^\cdot OH$$

$$h_{VB}^+/{}^\cdot OH + RhB \rightarrow CO_2 + H_2O$$

4.   Conclusion

In summary, Zn-doped TiO$_2$ nanoparticles with highly exposed (001) facets were synthesized by a one-step hydrothermal method. The photocatalytic activity of RhB degradation over the Zn-TiO$_2$(001) photocatalysts reaches 98.7% after 60 min of visible light irradiation. Zn doping effectively enhances the concentration of O vacancies and accelerates the formation of

hole and hydroxyl radicals from the generated electron–hole pairs and special crystal facet structure exposes more holes on the surface of TiO_2, which could contribute to the enhanced photocatalytic activity. The facile preparation method and outstanding photocatalytic performance provide a promising photocatalyst for organic pollutant degradation.

Conflicts of interest

There are no conflicts to declare.

Acknowledgements

Notes and references

1 J. Ji, Y. Xu, H. B. Huang, M. He, S. L. Liu, G. Y. Liu, R. J. Xie, Q. Y. Feng, Y. J. Shu, Y. J. Zhan, R. M. Fang, X. G. Ye and D. Y. C. Leung, *Chem. Eng. J.*, 2017, **327**, 490–499.

2 F. V. S. Lopes, R. A. R. Monteiro, A. M. T. Silva, G. V. Silva, J. L. Faria, A. M. Mendes, V. J. P. Vilar and R. A. R. Boaventura, *Chem. Eng. J.*, 2012, **204**, 244–257.

3 V. Kurnaravel, S. Mathew, J. Bartlett and S. C. Pillai, *Appl. Catal., B*, 2019, **244**, 1021–1064.

4 K. Wetchakun, N. Wetchakun and S. Sakulsermsuk, *J. Ind. Eng. Chem.*, 2019, **71**, 19–49.

5 M. Z. Ge, J. S. Cai, J. Iocozzia, C. Y. Cao, J. Y. Huang, X. N. Zhang, J. L. Shen, S. C. Wang, S. N. Zhang, K. Q. Zhang, Y. K. Lai and Z. Q. Lin, *Int. J. Hydrogen Energy*, 2017, **42**, 8418–8449.

6 S. Kohtani, A. Kawashima and H. Miyabe, *Catalysts*, 2017, **7**(10), 303.

7 C. Burda, Y. B. Lou, X. B. Chen, A. C. S. Samia, J. Stout and J. L. Gole, *Nano Lett.*, 2003, **3**, 1049–1051.

8 S. Sakthivel and H. Kisch, *ChemPhysChem*, 2003, **4**, 487–490.

9 M. Batzill, E. H. Morales and U. Diebold, *Phys. Rev. Lett.*, 2006, **96**, 4.

10 S. U. M. Khan, M. Al-Shahry and W. B. Ingler, *Science*, 2002, **297**, 2243–2245.

11 K. Bhattacharyya, J. Majeed, K. K. Dey, P. Ayyub, A. K. Tyagi and S. R. Bharadwaj, *J. Phys. Chem. C*, 2014, **118**, 15946–15962.

12 K. Bhattacharyya, B. Modak, C. Nayak, R. G. Nair, D. Bhattacharyya, S. N. Jha and A. K. Tripathi, *New J. Chem.*, 2020, **44**, 8559–8571.

13 K. Bhattacharyya, S. Varma, A. K. Tripathi, S. R. Bharadwaj and A. K. Tyagi, *J. Phys. Chem. C*, 2008, **112**, 19102–19112.

14 V. Moradi, M. B. G. Jun, A. Blackburn and R. A. Herring, *Appl. Surf. Sci.*, 2018, **427**, 791–799.

15 F. F. Wang, T. Shen, Z. P. Fu, Y. L. Lu and C. X. Chen, *Nanotechnology*, 2018, **29**, 7.

16 R. Camarillo, D. Rizaldos, C. Jimenez, F. Martinez and J. Rincon, *J. Supercrit. Fluids*, 2019, **147**, 70–80.

17 A. Heidarpour, Y. Mazaheri, M. Roknian and S. Ghasemi, *J. Alloys Compd.*, 2019, **783**, 886–897.

18 Y. Yu, J. Wang, W. Li, W. Zheng and Y. Cao, *CrystEngComm*, 2015, **17**, 5074–5080.

19 J. Li, J. Xu, W.-L. Dai, H. Li and K. Fan, *Appl. Catal., B*, 2009, **85**, 162–170.

20 A. Kudo, H. Kato and I. Tsuji, *Chem. Lett.*, 2004, **33**, 1534–1539.

21 S. Sun, W. Wang, L. Zhang, M. Shang and L. Wang, *Catal. Commun.*, 2009, **11**, 290–293.

22 M. Jakob, H. Levanon and P. V. Kamat, *Nano Lett.*, 2003, **3**, 353–358.

23 A. Y. Meng, J. Zhang, D. F. Xu, B. Cheng and J. G. Yu, *Appl. Catal., B*, 2016, **198**, 286–294.

24 M. Y. Xing, B. X. Yang, H. Yu, B. Z. Tian, S. Bagwasi, J. L. Zhang and X. Q. Gongs, *J. Phys. Chem. Lett.*, 2013, **4**, 3910–3917.

25 J. G. Yu, J. X. Low, W. Xiao, P. Zhou and M. Jaroniec, *J. Am. Chem. Soc.*, 2014, **136**, 8839–8842.

26 H. G. Yang, C. H. Sun, S. Z. Qiao, J. Zou, G. Liu, S. C. Smith, H. M. Cheng and G. Q. Lu, *Nature*, 2008, **453**(7195), 638–641.

27 Q. J. Xiang, K. L. Lv and J. G. Yu, *Appl. Catal., B*, 2010, **96**, 557–564.

28 Z. Wang, Y. Gu, J. Qi, S. Lu, P. Li, P. Lin and Y. Zhang, *RSC Adv.*, 2015, **5**, 42075–42080.

29 K. Bhattacharyya, A. Danon, B. K. Vijayan, K. A. Gray, P. C. Stair and E. Weitz, *J. Phys. Chem. C*, 2013, **117**, 12661–12678.

30 R. G. Nair, S. Mazumdar, B. Modak, R. Bapat, P. Ayyub and K. Bhattacharyya, *J. Photochem. Photobiol., A*, 2017, **345**, 36–53.

31 J. C. Yu, J. G. Yu, W. K. Ho, Z. T. Jiang and L. Z. Zhang, *Chem. Mater.*, 2002, **14**, 3808–3816.

32 J. Yu, W. Wang, B. Cheng and B.-L. Su, *J. Phys. Chem. C*, 2009, **113**, 6743–6750.

33 H. G. Yang, G. Liu, S. Z. Qiao, C. H. Sun, Y. G. Jin, S. C. Smith, J. Zou, H. M. Cheng and G. Q. Lu, *J. Am. Chem. Soc.*, 2009, **131**, 4078–4083.

34 L. F. Cui, T. T. Pu, Z. F. Shen, S. S. Li, S. F. Kang, Q. N. Xia, Y. G. Wang and X. Li, *Res. Chem. Intermed.*, 2019, **45**, 2167–2177.

35 H. N. Huang, H. L. Li, Z. Y. Wang, P. Wang, Z. K. Zheng, Y. Y. Liu, Y. Dai, Y. J. Li and B. B. Huang, *Chem. Eng. J.*, 2019, **361**, 1089–1097.

36 K. Rabe, L. F. Liu, N. A. Nahyoon, Y. Z. Zhang, A. M. Idris, J. Q. Sun and L. X. Yuan, *J. Taiwan Inst. Chem. Eng.*, 2019, **96**, 463–472.

37 Z. D. Liu, X. N. Liu, Q. F. Lu, Q. Y. Wang and Z. Ma, *J. Taiwan Inst. Chem. Eng.*, 2019, **96**, 214–222.

38 J. Zhang, J. Chen, Y. Wan, H. Liu, W. Chen, G. Wang and R. Wang, *ACS Appl. Mater. Interfaces*, 2020, **12**, 13805–13812.